nature biomedical engineering

ARTICLES

https://doi.org/10.1038/s41551-018-0271-5

A tissue-engineered scale model of the heart ventricle

Luke A. MacQueen[1,2], Sean P. Sheehy[1,2], Christophe O. Chantre[1,2], John F. Zimmerman[1,2], Francesco S. Pasqualini[1,2], Xujie Liu[3], Josue A. Goss[1,2], Patrick H. Campbell[1,2], Grant M. Gonzalez[1,2], Sung-Jin Park[1,2], Andrew K. Capulli[1,2], John P. Ferrier[1,2], T. Fettah Kosar[1], L. Mahadevan[1,2,4,5,6], William T. Pu[3,7] and Kevin Kit Parker[1,2,7]*

Laboratory studies of the heart use cell and tissue cultures to dissect heart function yet rely on animal models to measure pressure and volume dynamics. Here, we report tissue-engineered scale models of the human left ventricle, made of nanofibrous scaffolds that promote native-like anisotropic myocardial tissue genesis and chamber-level contractile function. Incorporating neonatal rat ventricular myocytes or cardiomyocytes derived from human induced pluripotent stem cells, the tissue-engineered ventricles have a diastolic chamber volume of ~500 µl (comparable to that of the native rat ventricle and approximately 1/250 the size of the human ventricle), and ejection fractions and contractile work 50–250 times smaller and 10^4–10^8 times smaller than the corresponding values for rodent and human ventricles, respectively. We also measured tissue coverage and alignment, calcium-transient propagation and pressure–volume loops in the presence or absence of test compounds. Moreover, we describe an instrumented bioreactor with ventricular-assist capabilities, and provide a proof-of-concept disease model of structural arrhythmia. The model ventricles can be evaluated with the same assays used in animal models and in clinical settings.

Laboratory models of the heart are used to gain a mechanistic understanding of heart function in health and disease, and to test the safety and efficacy of potential therapeutics. The heart is studied at multiple scales in vitro, from cellular assays to excised or engineered tissues and 'organ-on-chip' microphysiological systems[1] that recapitulate integrated aspects of specific pathological conditions. Functional readouts obtained using engineered heart tissues include contractile forces and electrophysiological measurements[2], but direct comparison with natural ventricle pressure and volume dynamics requires three-dimensional (3D) contractile cardiac chambers. To obtain these measurements, animal models and isolated heart preparations are evaluated using preclinical and clinical measurement modalities such as catheterization[3], echocardiography[4], and magnetic resonance imaging[5]. Data obtained using these methods allow direct comparison with patient data, but differences in genetics, physiology and disease aetiology limit the utility of animal models for developing therapeutic interventions[6,7]. These and other limitations associated with animal models, for example, high maintenance costs and low experimental throughput, motivate the development of alternative in vitro cardiology assays based on human cells.

Human induced pluripotent stem cell-derived cardiomyocytes (hiPSC-CMs) have emerged as a promising tool for in vitro cardiology, with the potential to eliminate interspecies and interpersonal variations through patient-specific derivation[8]. These cells are assembled into functional engineered heart tissues[2,9,10], including muscular thin films[11,12] or 3D muscle strips[13–20], to model contractile pathophysiologies[11], promote hiPSC-CM maturation[9,14,15,21] and produce drug responses that are increasingly comparable to human patients[16,18,22]. However, the lack of in vitro models based on hiPSC-CMs that accurately reproduce the architecture and functional output of the heart chambers[9,10,23] is a significant limitation because tissue performance cannot be directly compared with animal or human heart performance, which are evaluated by measuring changes in chamber pressure and volume[24,25]. Engineered cardiac organoid chambers comprising cardiomyocytes embedded in isotropic hydrogels show significant promise for obtaining intraventricular pressure measurements[26–29], but the lack of a scaffold to guide cell assembly hampers the formation of organized tissues that recapitulate the laminar architecture[30,31] of the native myocardium. Instead, we decided to use 3D scaffolds to provide anisotropic cues that guide the same laminar tissue formation we obtained on patterned monolayers[32–35] and extend these design rules to tissues composed of multiple cell layers. Based on reports describing anisotropic cardiomyocyte assembly in fibrous scaffolds[36–39], we reasoned that by taking design inspiration from the human myocardial tissue architecture and recreating it using a nanofibre production system, we could build 3D tissue-engineered ventricle scaffolds. Nanofibres provide biochemical and nanotopographical structural cues with sufficient fidelity to guide cell adhesion, orientation, shape and assembly[40,41]. We therefore hypothesized that ventricle-shaped nanofibrous scaffolds would promote cardiomyocyte assembly into functional 3D tissue-engineered ventricle chambers.

To test whether nanofibrous scaffolds are suitable for ventricle chamber tissue engineering, we first determined the minimal essential features of human ventricle structure that can be reliably recapitulated using nanofibre production systems. We fabricated ellipsoidal thin-walled chambers composed of a nanofibrous synthetic–natural

[1]Wyss Institute for Biologically Inspired Engineering, Harvard University, Boston, MA, USA. [2]John A. Paulson School of Engineering and Applied Sciences, Harvard University, Cambridge, MA, USA. [3]Department of Cardiology, Boston Children's Hospital, Boston, MA, USA. [4]Kavli Institute for Bionano Science and Technology, Harvard University, Cambridge, MA, USA. [5]Department of Organismic and Evolutionary Biology, Harvard University, Cambridge, MA, USA. [6]Department of Physics, Harvard University, Cambridge, MA, USA. [7]Harvard Stem Cell Institute, Harvard University, Cambridge, MA, USA. *e-mail: kkparker@seas.harvard.edu

polymer–protein blend and seeded them with neonatal rat ventricular myocytes (NRVMs) or hiPSC-CMs. Synchronous chamber-level contraction was observed for both cell types after three to five days of culture in the scaffolds. The resulting tissue-engineered ventricle chambers were sutured to tubing or bioreactor components through which catheter sensors were introduced and stable contraction of both NRVM and hiPSC-CM ventricles permitted time-dependent pressure and volume measurements. We then provide a proof-of-concept structural arrhythmia disease model by measuring spontaneous calcium activity of an engineered rat ventricle before and after inflicting geometrically controlled injuries. Our findings confirm that tissue-engineered model ventricle contraction can be monitored by catheter sensors, and suggest that model ventricles are suitable for cardiac arrhythmia studies. These results have implications for preclinical cardiology and regenerative medicine research where human organ models are sought to improve translation of therapeutic strategies.

Model assumptions for tissue-engineered ventricle chambers

To begin, we developed a model cardiac chamber based on tabulated structural and functional properties of the human left ventricle[40]. In the native heart, overlapping myocardial fibres are arranged into distinct laminae four to six myocytes thick and separated from adjacent laminae by an extracellular collagen network[42]. We reasoned that we could recapitulate the structure of model myocardial laminae within an ellipsoidal chamber geometry. Our overall strategy to produce a scale model of the human left ventricle chamber for pressure–volume catheterization is depicted schematically in Fig. 1a. We made the following assumptions from the outset: (1) we would build a scale model of the human left ventricle chamber with a diastolic chamber volume of ~500 µl (~2× rat, ~1/250 human); (2) the ventricle wall would not be vascularized and its thickness limited to ~0.1 mm (~1/10 rat, ~1/100 human) to maintain high cell viability within the diffusion-limited environment; (3) the ventricle scaffold material would be a well-known protein–polymer mixture to ensure production reproducibility using existing nanofibre systems; and (4) cardiomyocyte alignment would be circumferential throughout the scaffold, representing a thin-walled approximation of the helical alignment within the native ventricular wall.

Ventricle scaffold

Healthy ventricular musculature (myocardium) arises from precisely coordinated multiscale integration of physical forces transmitted between cells and the extracellular matrix (ECM), as well as between neighbouring cells[43]. The myocardial ECM is fibrillar and anisotropic, and provides nanotopographical cues that guide cardiomyocyte alignment and assembly[44], ultimately forming a helicoid structure that optimizes ejection fraction during ventricular contraction[45]. These features can be recapitulated using nanofibrous materials that are formed into cellular scaffolds with sufficient porosity to support cell infiltration and promote tissue morphogenesis[40]. We therefore developed a nanofibre ventricle chamber production strategy based on pull -spinning[46] fibres on a rotating ellipsoidal collector (Fig. 1b, Supplementary Fig. 1, Supplementary Video 1), which ensures roughly circumferential fibre alignment (Fig. 1c and Supplementary Video 2). We selected polycaprolactone (PCL)/gelatin nanofibres as our material of choice because they are biocompatible and biodegradable, they promote cell adhesion, provide sufficient structural integrity for ventricle culture and catheterization, and can be produced by a variety of nanofibre production systems that include electrospinning and force-spinning methods[40]. PCL provides structural stability for the scaffold's nanofibrous features during culture, while gelatin was chosen as an arginyl-glycyl-aspartic-acid-containing biopolymer derived from denatured collagen that improves scaffold binding to cells and biomolecules such as fibronectin[47,48]. We previously described anisotropic PCL/gelatin nanofibre production by pull spinning and their use to guide skeletal muscle tissue assembly[46]. Here, we used scanning electron microscopy (SEM) to confirm that PCL/gelatin nanofibre scaffolds were structurally comparable with decellularized human left ventricle tissue (Supplementary Fig. 2a). Gelatin incorporated into the nanofibres persisted for at least four days in aqueous solutions according to measurements made using X-ray photoelectron spectroscopy (Supplementary Fig. 2b). The tensile elastic modulus of our scaffolds was anisotropic, with values measured longitudinally (in the direction parallel to the fibre axis), $E_L = 500 \pm 31$ kPa, or transverse (in the direction perpendicular to the fibre axis), $E_T = 74 \pm 15$ kPa (Supplementary Fig. 2c). These properties allowed us to fabricate ventricle scaffolds that were both structurally stable and permissive to chamber contraction by cardiomyocyte shortening.

Given that natural contraction rates of cultured cardiomyocytes are ~60–120 bpm (~1–2 Hz)[16,49], we designed chamber scaffolds that were mechanically permissive to contraction in the same range. To estimate the scaffold resonant bending frequency, ω_B, we considered a simple balance between the kinetic and potential energy of a thin fluid-loaded spherical elastic shell of modulus, E, radius, R, fluid density, ρ_f and thickness, h (ref. [50]). The kinetic energy associated with the wall motion of amplitude, A, and frequency, ω_B, scales as $\rho_f R^3 A^2 \omega_B^2$. The potential energy of deforming the shell is dominated by long wavelength bending deformations and scales as $Eh^3 (A/R^2)^2 R^2$, where Eh^3 is the bending stiffness, and the curvature scales as A/R^2. Balancing the two yields $Eh^3(A^2/R^2) \sim \rho_f A^2 R^3 \omega_B^2$ so that $\omega_B \sim \sqrt{(Eh^3/\rho_f R^5)}$. Using parameter values from our scaffolds ($R = 5$ mm, $h = 0.1$ mm, $50\,\text{kPa} < E < 500\,\text{kPa}$) gives bending resonant frequencies of $0.67\,\text{Hz} < f_B < 2\,\text{Hz}$, where $f_B = \omega_B / 2\pi$, which match the contraction rates of cardiomyocytes. This suggests a natural design principle to engineer artificial ventricles as a function of the natural frequencies of cardiomyocyte contraction.

Tissue-engineered ventricle chamber

To build our model ventricle chambers, we seeded ventricle-shaped scaffolds with either NRVMs or hiPSC-CMs. Synchronous, coordinated ventricle contraction developed spontaneously after three to five days of culture (Supplementary Videos 3 and 4) and persisted for the duration of experimental procedures (Supplementary Video 5), conducted fourteen days after seeding. Calcium imaging, which has been used as a surrogate for the action potential[51], revealed continuous excitation propagation on the ventricle surfaces, confirming electrical continuity throughout the ventricle constructs (Fig. 1d and Supplementary Videos 6 and 7). Mean calcium wavefront propagation velocity from apex to base was 9.33 cm s^{-1} or 5.2 cm s^{-1} for NRVM or hiPSC-CM ventricles, respectively. These values are comparable to those observed in tissues composed of immature cells where cell geometry, calcium handling, gap junction expression and spatial distribution, as well as other factors limit the conduction velocity when compared with mature tissues[52,53]. Immunostaining confirmed fibre-directed anisotropic cell alignment and infiltration within the chamber wall (Fig. 2, Supplementary Figs 3 and 4, and Supplementary Video 8), enabling us to quantify cell alignment using a metric known as the orientational order parameter (OOP) that ranges from zero (random organization) to one (perfect alignment)[35,54]. Both NRVM and hiPSC-CM ventricles showed high alignment based on OOP analysis of F-actin stains (Supplementary Fig. C), with OOP values of 0.84 ± 0.02 (NRVM) and 0.85 ± 0.02 (hiPSC-CM).

Intraventricular pressure and volume measurements

To determine whether our engineered ventricles exhibited in vivo-like chamber contraction, we measured time-dependent intraventricular pressure and volume by catheterization (Fig. 3 and Supplementary Fig. 5), an established method for heart chamber performance evaluation[25]. We sutured the engineered ventricles around tubing and inserted a pressure–volume (PV) catheter into

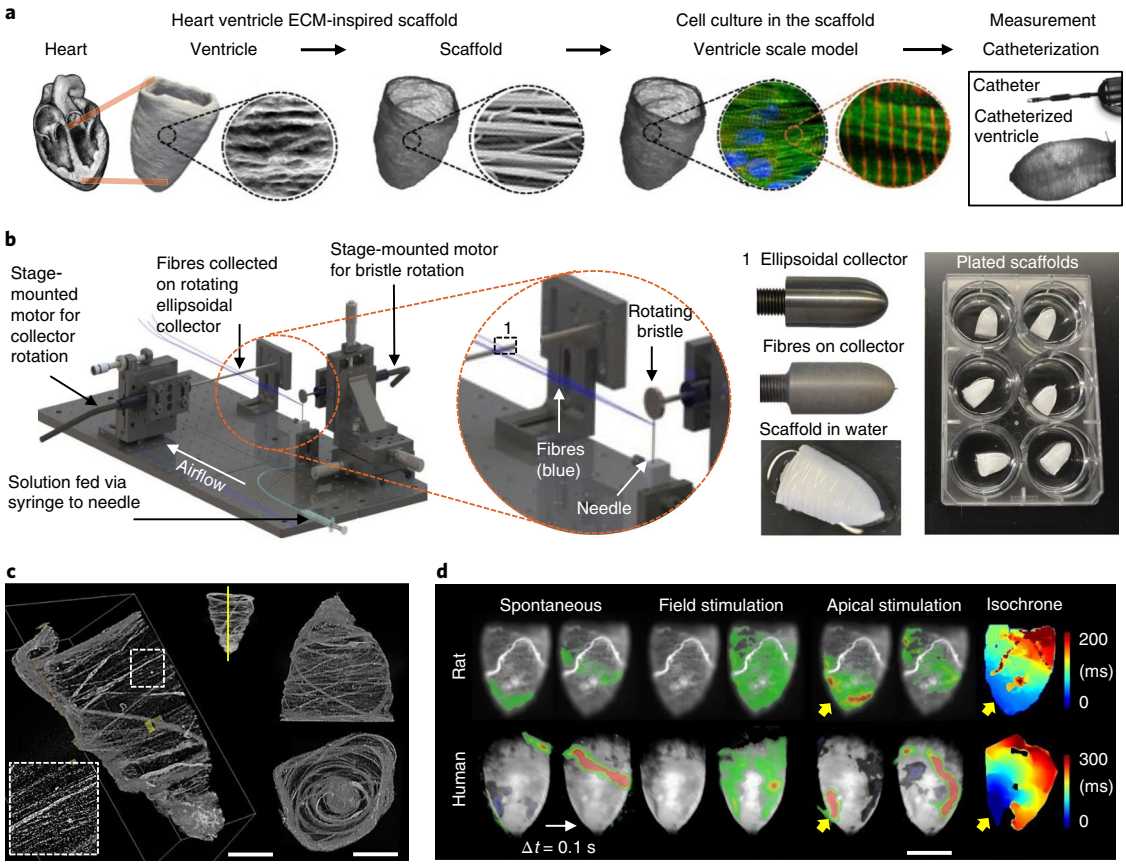

Fig. 1 | Tissue-engineered model ventricles recapitulate key structural and functional aspects of natural ventricular myocardium. a, A schematic overview of the ventricle design–build–test project phases, from left to right. Human left ventricle ellipsoidal shape and fibrous ECM inspired our use of circumferentially oriented nanofibres in scale-model ellipsoidal ventricle scaffolds. We seeded these scaffolds with cardiomyocytes to produce tissue-engineered ventricles and evaluated their contractile strength by pressure–volume catheterization. **b**, Pull spinning a nanofibrous ellipsoidal model ventricle scaffold. A high-speed rotating bristle dips into a fixed, continuous polymer source that is fed via a syringe pump through a small orifice (in this case a needle). The bristle pulls the polymer column into a polymer jet that is ejected towards a rotating collector. Solvent evaporation occurs as the polymer jet travels towards the collection mandrel, where the resulting nanofibres are collected. The resulting ventricle scaffolds are removed from the collector by tweezers in a hydration bath. **c**, Microcomputed tomography images of a ventricle scaffold. Scale bars, 10 mm (left); 5 mm (right). **d**, Calcium propagation imaging performed on day 14. Left: spontaneous activity produced propagating waves but they did not always originate at the apex. Middle: field stimulation, resulting from electrical pacing where electrodes were placed far from the ventricle surface, produced uniform calcium activation. Right: apical point stimulation (indicated by yellow arrows) produced calcium waves that propagated from apex to base at a rate of 9.33 cm s^{-1} for NRVM ventricles and 5.2 cm s^{-1} for hiPSC-CM ventricles (right). Calcium fluorescence intensity is displayed as a heat map ranging from blue (minimum) to red (maximum), overlaid on a greyscale image of the ventricle surface. Scale bar, 10 mm.

the chamber midway from base to apex (Supplementary Fig. 5a). We performed catheter calibrations (Supplementary Fig. 5) and acquired 2,000 data points per second (Supplementary Fig. 6). Exported data were processed for time- and frequency-domain analyses, which are commonly used to quantitatively assess cardiovascular function[55,56] (Supplementary Fig. 7). As an initial validation of our experimental system, we investigated ventricle contractile responses to gross alterations in the composition of the extracellular bath solution. Whereas regular beat frequencies were observed in calcium-containing M199 or Tyrode's solution, exposure to calcium-free PBS led to broad beat-rate distributions (Supplementary Fig. 7b). Furthermore, we observed an expected reduction in beat rate, as judged by a shift in the frequency spectrum, as bath temperature was decreased from physiological 37 °C to less than ~30 °C (Supplementary Fig. 7c). These results demonstrate that tissue-engineered model ventricles can be functionally interrogated and myocardial performance assessed using catheter-based PV measuring systems. To visualize the relationship between pressure and volume change during cardiac contraction cycles, we plotted PV loops for both rat (NRVM) and human (hiPSC-CM) ventricles from PV catheter measurements (Fig. 3b). Measured differences in chamber pressure were ~50 μmHg (rat or human) and the volume change was ~5 μl (rat) or 1 μl (human). Thus, ejection fractions were ~1% (rat) or ~0.2% (human) and stroke work was $W_S \sim 0.25$ mmHg × μl (rat) or $W_S \sim 0.05$ mmHg × μl (human).

A fundamental aspect of myocardial function is the response to adrenergic agonists, which has been studied extensively in both rodents and humans, making β-adrenergic response a good test of the ability of our engineered ventricles to recapitulate normal cardiac pharmacology[57,58]. To assess the chronotropic response of our engineered ventricles to a β-adrenergic receptor agonist, we subjected them to concentrations of isoproterenol ranging from 0.1 nM to 0.1 mM. PV loops measured before and after isoproterenol exposure showed an isoproterenol-induced reduction in stroke work, concomitant with an increase in beat frequency (Fig. 3b,c). Continuous intraventricular pressure and volume measurements enabled frequency-domain analysis of the chronotropic response of either NRVM or hiPSC-CM ventricles (Supplementary Fig. 7d). The spontaneous beat rate of NRVM ventricles (~130 ± 15 bpm) was higher than hiPSC-CM ventricles (~85 ± 15 bpm), and both

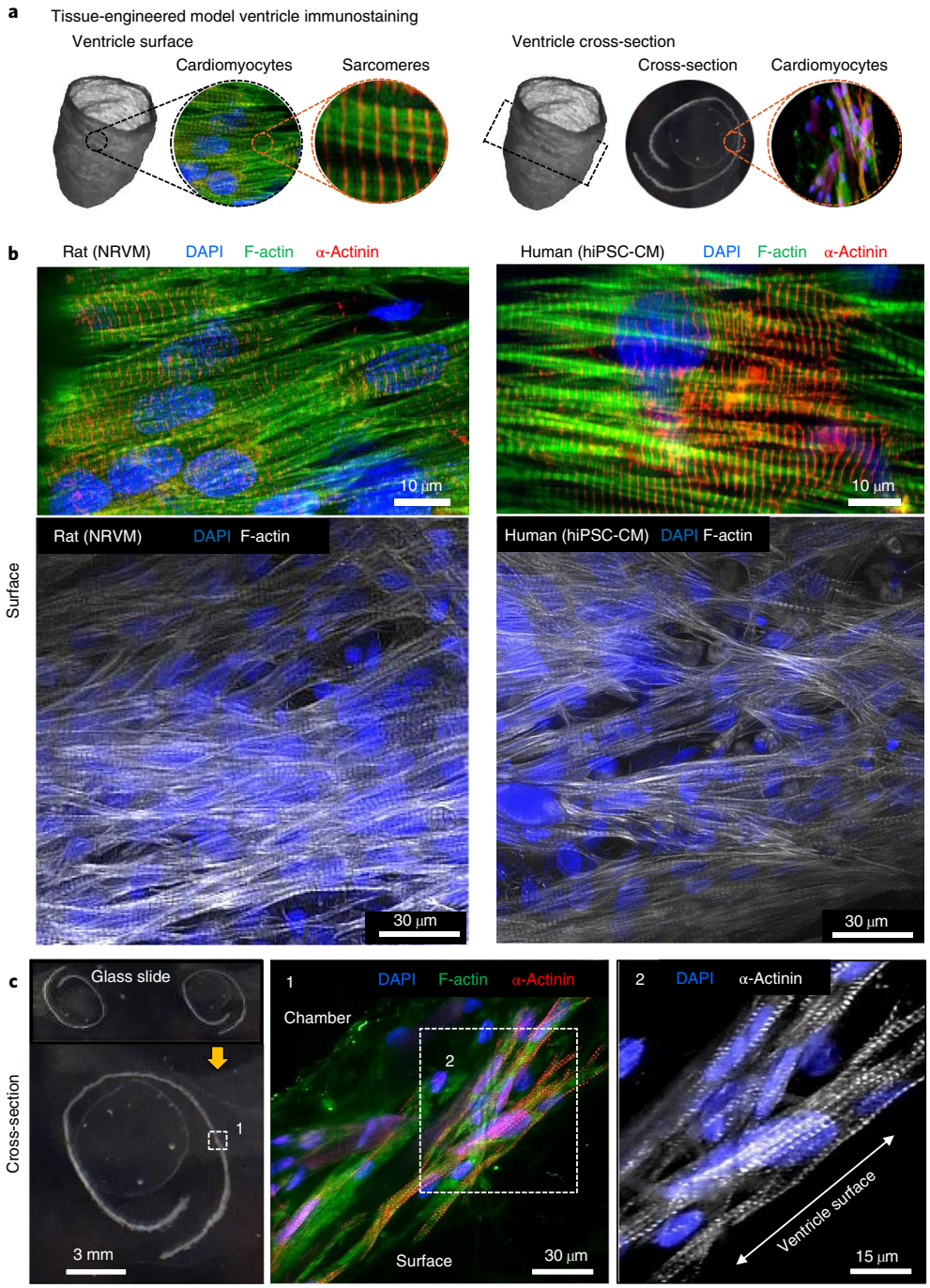

Fig. 2 | Tissue-engineered ventricle immunostaining. a, Schematics of ventricle surface and cross-section immunostains. **b**,**c**, Surface (**b**) and cross-section (**c**) immunostains. In all cases, cells were introduced via the exterior surface and imaging was performed following 14 days in culture. Immunostaining confirmed that both NRVMs and Cor.4U hiPSC-CMs infiltrated the scaffolds and were aligned roughly circumferentially, coincident with the scaffold's nanofibre ultrastructure. Images in **c** are rat only.

increased by ~40% following exposure to 10^{-4} M isoproterenol. Ventricle beat rates showed a positive chronotropic response over the concentration range in both the NRVM and hiPSC-CM ventricles (Fig. 3c), as expected for healthy NRVM[59], hiPSC-CM[60], engineered hiPSC-CM cardiac tissues[16] and human patients[61].

Bioreactor for modular assembly of ventricles and valves

Laboratory models of biological tissues often benefit from culture in bioreactors or microfluidic technologies where fluid exchange can be automated and in situ measurements obtained. To support tissue-engineered ventricle culture, we built a self-contained instrumented heart bioreactor (HBR; Fig. 4, Supplementary Figs 8 and 9, and Supplementary Video 9). The HBR includes both intra- and extraventricular flow loops, separate chambers for optional valve inserts and additional access ports for catheters (Fig. 4a and Supplementary Fig. 8). Cyclic pressure applied to the extraventricular loop drives intraventricular fluid flow via assisted ventricle contraction, and unidirectional flow can be achieved using commercially available valves or with custom valve inserts in the HBR. We demonstrated assisted pumping in the absence of drugs by

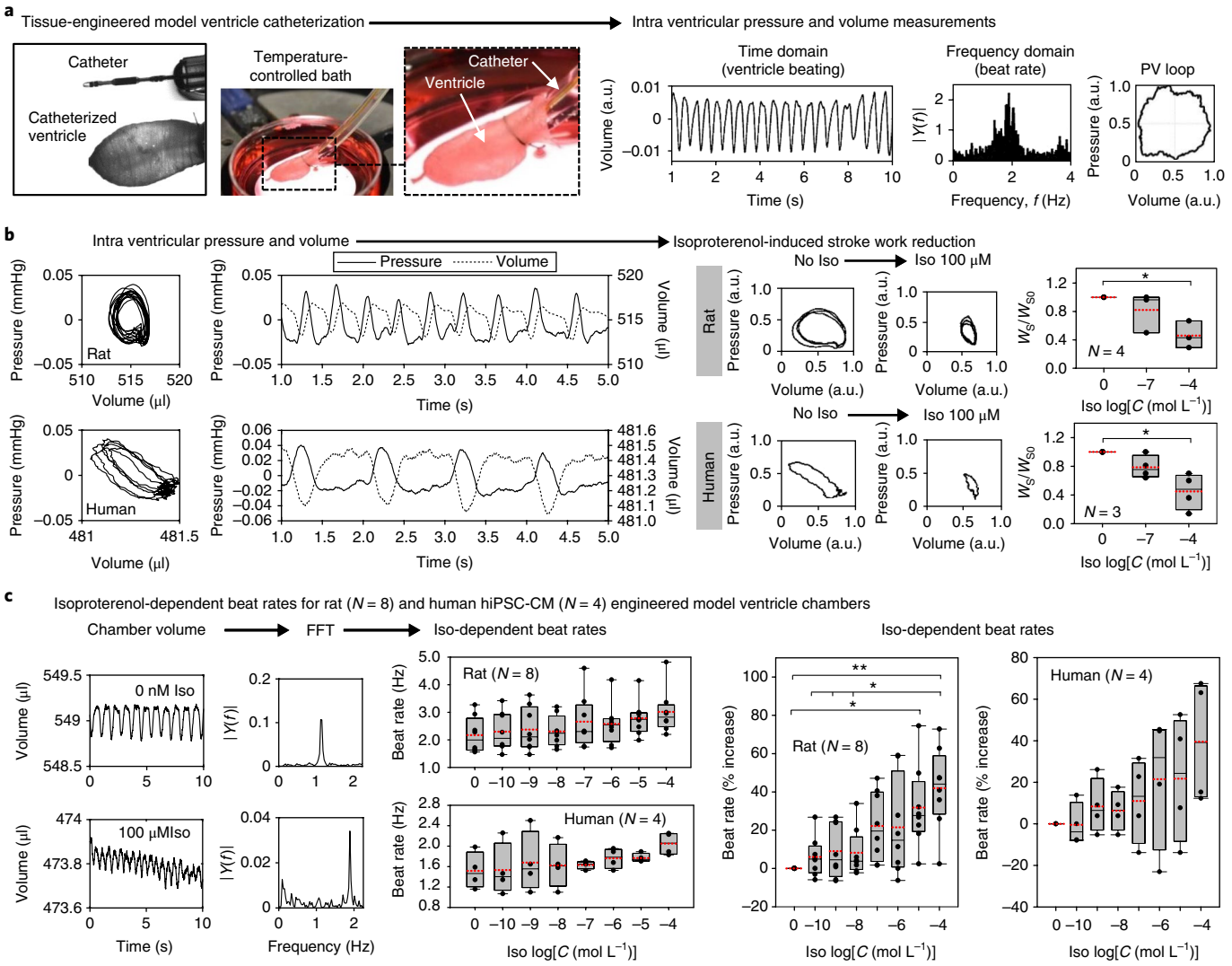

Fig. 3 | Intraventricular PV data obtained by tissue-engineered ventricle catheterization. a, An overview of the ventricle catheterization procedure. Catheters were fed through tubing on which the ventricle base was sutured. Ventricles were submerged within a 3.5 cm Petri dish bath, which was mounted on a temperature-controlled heating stage. Catheter readouts fed to signal amplification instruments provided real-time measurements of intraventricular pressure and volume. *Y*, single-sided amplitude spectrum of the fast Fourier transformation. **b**, Intraventricular pressure and volume measured by catheterization of NRVM- or Cor.4U hiPSC-CM-based ventricles. Exposure to isoproterenol (Iso) reduced stroke work of both rat and human ventricles. Here, pressure and volume were normalized by polynomial fit to remove measurement drift occurring over the course of multiple Iso doses.*$P < 0.05$; *P* values were $P = 0.04$ (NRVM, $N = 4$ ventricles) and $P = 0.038$ (Cor.4U, $N = 3$ ventricles). *C*, isoproterenol concentration. **c**, Iso-dependent beat rates for rat ($N = 8$ ventricles) and human ($N = 4$ ventricles). Time-domain recordings of chamber volume were Fourier-transformed (FFT) to obtain beat rates. The spontaneous beat rate of NRVM ventricles (~130 ± 15 bpm) was higher than hiPSC-CM ventricles (~85 ± 15 bpm), and both increased by ~40% following exposure to 10^{-4} M Iso. *$P < 0.05$, **$P < 0.001$, compared with baseline (no Iso), one-way ANOVA with Tukey post-hoc test. Exact *P* values for Iso-dependent beat rates (Hz) were $P = 0.0325$ (NRVM, $N = 8$ ventricles) and $P = 0.524$ (Cor.4U, $N = 4$ ventricles). Exact *P* values for Iso-dependent beat rate (% increase) were $P < 0.001$ for baseline NRVM versus the highest Iso dose of 10^{-4} M. Exact *P* values for NRVM at the smallest three doses (10^{-10} M, 10^{-9} M and 10^{-8} M Iso) versus the largest dose (10^{-4} M Iso) were $P = 0.003$, $P = 0.006$ and $P = 0.008$, respectively. The exact *P* value for NRVM dosed with 10^{-9} M Iso versus 10^{-4} M Iso was $P = 0.011$. For Cor.4U, differences in beat rate were not statistically significant ($P = 0.183$). In all cases, measurements were performed on day 14. Data are presented as box plots with individual data points overlaid, where lower or upper edges of the box represent 25th or 75th percentiles, the middle bar is the median, dashed red bar is the mean, and whiskers are minimum and maximum values.

controlling pressure delivered to the external (assist) channel using a pressure-driven programmable pump and cast-moulded silicone tricuspid valves to direct flow (Fig. 4a and Supplementary Fig. 9). In this configuration, cultured ventricles can be exposed to externally controlled physiological or pathological pressure variations and PV loops acquired with or without valves (Fig. 4b), emphasizing the potential to study heart failure where differential effects of various organ substructures are measured. Lastly, to highlight the translational nature of this technology, we monitored ventricle contraction by ultrasound through removable elastomeric windows in the HBR (Fig. 4c, Supplementary Fig. 10, Supplementary Videos 10 and 11). Using small animal echocardiography equipment, we recorded both unassisted natural spontaneous ventricle contraction (Fig. 4c, left, and Supplementary Video 10) and HBR-assisted contraction (Fig. 4c, right, and Supplementary Video 11). Echocardiography performed in the absence of extraventricular tissues can improve image clarity compared with in vivo studies, underscoring the advantage of organ modularity in our HBR.

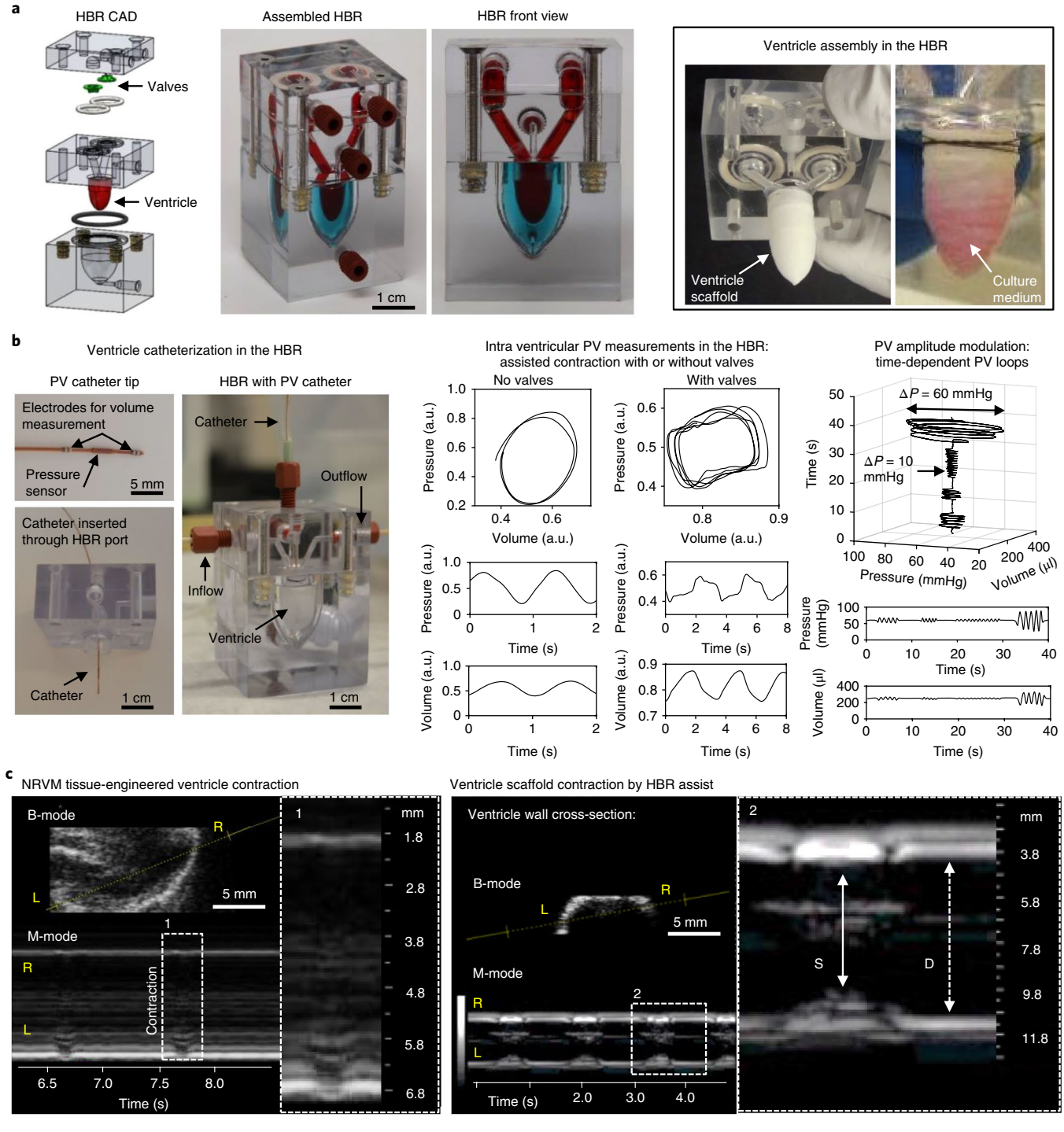

Fig. 4 | A HBR for tissue-engineered ventricle culture, assisted contraction and instrumentation. a, An overview of ventricle and valve (optional) assembly within the HBR. A computer-aided design (CAD) drawing of HBR components shows valve and ventricle placement. The ventricle wall separates intra- and extraventricular flow loops, which are indicated by red and blue dyes in the assembled HBR. Ventricle scaffolds are sutured over a support ring where input and output channels of the intraventricular flow loop converge. Pressure supplied by an external source to the extraventricular flow loop drives assisted ventricle contraction and flow through the intraventricular flow loop. **b**, Ventricle catheterization in the HBR enabled pressure and volume measurements during assisted ventricle contraction with or without cast-moulded silicone tricuspid valves. **c**, Echocardiographic measurement of a tissue-engineered NRVM (day 14) ventricle contracting unassisted (left) and a cell-free ventricle scaffold contracting by HBR assist (right). In both cases, cross-sections (brightness mode) and time-dependent traces of the ventricle wall (motion, M-mode) are shown. L, left; R, right; S, systole; D, diastole.

Structural arrhythmia disease model

In myocardial tissues, anatomical structures can introduce heterogeneities of impulse conduction that lead to ventricular tachycardia, including spiral waves anchored to anatomical defects[33,62]. Here, we show a proof-of-concept structural arrhythmia disease model by measuring spontaneous calcium activity of an engineered rat (NRVM) ventricle before and after inflicting geometrically controlled (1 mm diameter) injuries (Fig. 5). Plane wave propagation was observed before injury (Fig. 5a, top), whereas injured ventricles generated spiral waves that were pinned to

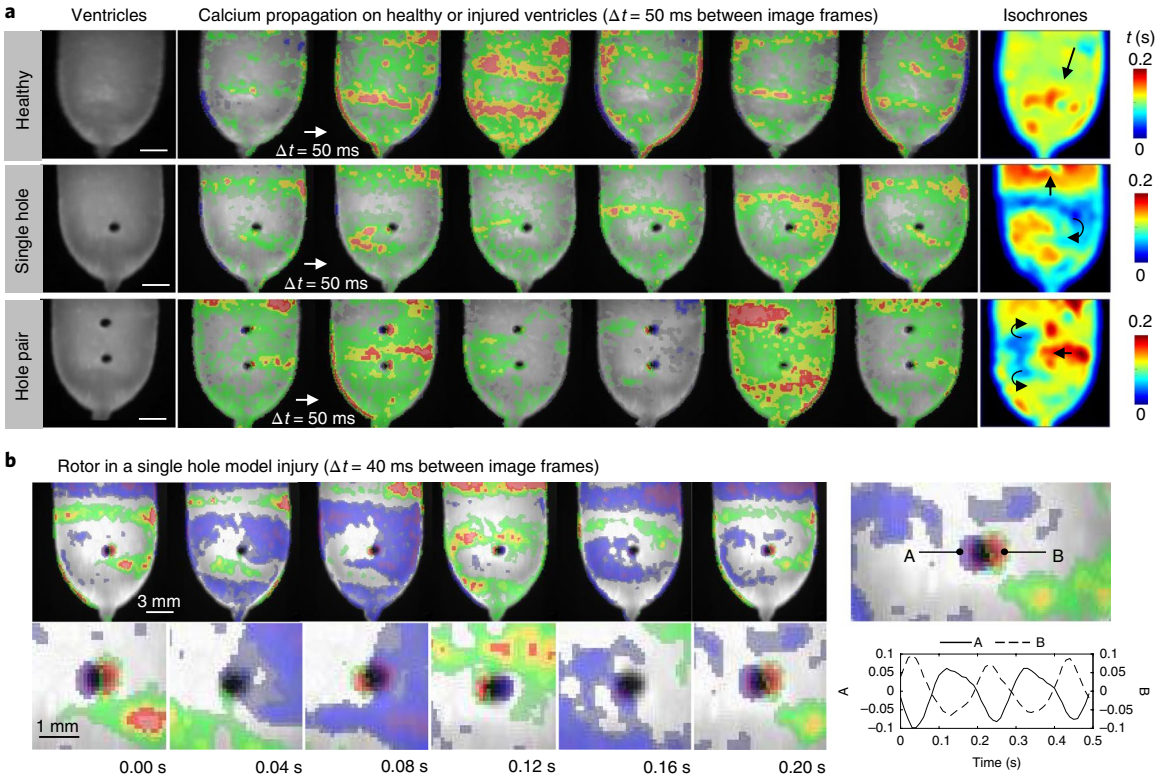

Fig. 5 | Structural arrhythmia disease model. a, Calcium wavefront propagation on a healthy (top) or injured (middle and bottom) tissue-engineered NRVM ventricle. The uninjured ventricle exhibited plane waves with a peak-to-peak spatial period of ~5 mm (top). Subsequent injury of this ventricle using a 1 mm diameter biopsy punch resulted in circular anatomical defects that generated pinned spiral waves. The single-hole injury (middle) generated a single spiral wave whereas the hole pair (bottom) generated counterpropagating spiral waves that converged and propagated through the inter-hole region with each cycle. Black arrows in isochrone images indicate direction of calcium wave rotation and propogation. Scale bars, 3 mm. **b**, Calcium fluorescence intensity measurements near the rotor poles of the single-hole injury showed consistent phase difference and a rotation rate of ~5 Hz. Experiments were performed at day 12 and spontaneous activity was recorded without external stimulation for all cases. Measurements shown in **a** were acquired using a 5 ms exposure window, whereas those shown in **b** were acquired using a 10 ms exposure window. In all cases, the temporal derivative of calcium fluorescence intensity is displayed as a heat map ranging from blue (minimum) to red (maximum), overlaid on a greyscale image of the ventricle surface. A and B (right) refer to points selected on opposite sides of the injury site. Graph in **b** shows time-dependent calcium intensity at points A and B, which are out of phase.

the controlled anatomical defects (Fig. 5a, bottom panels, and Supplementary Video 12). Calcium fluorescence intensity measured near the rotor poles of a single-hole injury model showed consistent phase difference and a rotation rate of ~5 Hz (Fig. 5b, Supplementary Fig. 12, and Supplementary Video 13). The two-hole injury generated counterpropagating spiral waves that merged within the region between holes (Fig. 5a, third row). In all cases, spontaneous calcium activity showed stable excitation patterns with plane waves (healthy) or pinned spiral waves (injured) repeating at a near-constant rate (between 4 and 5 Hz) for the duration of experiments (~2 h). These results suggest the feasibility of using tissue-engineered heart chambers to study arrhythmogenic heart diseases.

Discussion

Preclinical cardiology and regenerative medicine research will benefit from an expanding set of in vitro models where human heart structure and function are examined at multiple scales[2,9,10,63]. Here, we took inspiration from the myocardial ECM and used nanofibres to extend to 3D tissue-engineered cardiac chambers the same engineering design principles that led to increasingly functional laminar cardiac tissues[32,34,64]. For near-future design iterations that concentrate on myocardial engineering, we suggest several steps that may precede the addition of non-cardiomyocytes and ventricle vascularization[65]. These 'obstacles and opportunities' facing bioartificial hearts[66] include improvements to scaffolds, cardiomyocytes and culture protocols, briefly outlined below.

Scaffold engineering should account for the fact that the myocardium is a composite in which the dominant stiffness shifts from myocytes to the ECM with increasing strain[67], emphasizing the ECM's role maintaining structural integrity. In our scaffold, gelatin was used to enhance cell and biomolecule adhesion during cell seeding, and the polymer backbone (PCL) provided structural features (microporosity, nanotopography, anisotropy) that resisted degradation during culture. These features provided sufficient structural integrity for ventricle culture and they guided cardiomyocyte assembly, but alternative nanofibrous materials used for cardiac tissue engineering[40] may improve scaffold customization. For example, the tensile elastic modulus of our scaffold in the direction of fibre alignment (E_L ~ 500 kPa) was higher than healthy ventricular ECM (E ~ 350 kPa)[68] and may have limited cardiomyocyte shortening during contraction. The balance between structural support during culture, scaffold degradation rate and ventricle mechanics should be refined. Alternative biodegradable polymers or bioprotein mixtures reflecting age-dependent composition of natural myocardial ECM[40] may be used to improve scaffold elasticity, recapitulate specific disease or development phases, or promote scaffold replacement with cell-secreted ECM. Biomolecular nanofibres can be produced using precipitation systems[69] for direct use as scaffolds or dispersed in printable 'inks', where ink and print

conditions influence printed nanofibre orientation[70]. Our work suggests that including a nanofibrous component to printable inks would be advantageous for directing cardiomyocyte shape and assembly in printed scaffolds or tissues. Alternative chamber shapes, anatomical features and scaffold fibre alignments may be used to study their effects on cardiomyocyte assembly and electromechanical integration. In all cases, design rules for contractile 3D chambers should account for chamber contraction as a function of chamber size, shape and elastic modulus. Our calculations of resonant bending frequencies suggest a natural design principle to engineer cardiac chambers as a function of their intended beat rates.

Cardiomyocyte spontaneous beat rates in our model ventricles were similar to other in vitro assays based on NRVMs[49] or hiPSC-CMs[16], showing moderate positive chronotropy (~40% beat rate)[10,18]. We expected to observe variance between ventricles, both in terms of beat rates and their response to isoproterenol, given the heterogeneous pace-making phenotypes within the cardiomyocyte populations[10]. Our observation of isoproterenol-induced stroke work reduction (Fig. 3b) is consistent with negative force–frequency relationships observed in tissues based on immature cardiomyocytes, including NRVMs[71] and hiPSC-CMs[72]. The moderate positive chronotropy and reduction of stroke work observed at high isoproterenol doses are characteristic of immature tissues exhibiting poorly developed calcium handling properties[8], suggesting that maturation protocols[14,21,22,73] may be required to obtain positive force–frequency relationships, as observed in healthy adult human ventricular myocardium[74].

Critical to the advance of tissue-engineered ventricles will be the development of in situ stem cell proliferation, differentiation and maturation protocols. The cell density in our ventricles, estimated by counting immunostained (4,6-diamidino-2-phenylindole (DAPI)) NRVM ventricle surfaces and cross-sections (Supplementary Fig. 3), was ~90,000 cells mm^{-3} for a total cell number ~2.3×10^6 in a 26 mm^3 scaffold volume, which is approximately tenfold less than in 21-day-old or 3-month-old rat hearts[75]. The ejection fraction of our tissue-engineered rat ventricles was ~1% (1/50 ejection fraction of healthy rats), suggesting that discontinuities in cardiomyocyte coverage limited tissue-engineered ventricle contractile strength. Novel protocols that proliferate stem cells to confluence within the scaffolds may overcome the coverage limitation, provided that in situ differentiation and maturation can be efficiently achieved following the proliferation phase. Preliminary work in our laboratories suggests that we can achieve extended culture periods for NRVMs (Supplementary Fig. 12 and Supplementary Videos 14 and 15) and hiPSC-CMs (Supplementary Figs. 13 and 14) in our nanofibrous scaffolds. For example, proliferative hiPSC (line PGP1-iPSC) seeded in our scaffolds at a density of 10^5 cells cm^{-2} and cultured according to previously described protocols[11] achieved confluence within 4 days of culture (Supplementary Fig. 13a, day 0). When cultured in differentiation media, the resulting hiPSC-CM showed spontaneous contraction and early stages of sarcomeric assembly within 8–12 days of culture (Supplementary Fig. 13a, day 12), and anisotropic sarcomeric assembly with early stages of z-disk alignment after 1 month in culture (Supplementary Fig. 13a, day 30). We also cultured a non-proliferative hiPSC-CM line (Cor.4U) in model ventricle scaffolds for 6 months, demonstrating that tissue anisotropy was preserved (Supplementary Fig. 14a) and stable PV loops could be recorded (Supplementary Fig. 14b). These preliminary results suggest that our scaffolds support functional myocardial tissue production using relatively small numbers of seeded hiPSC that can subsequently be cultured for extended time periods. In these cases, tissue maturation may benefit from bioreactor culture where tissues are exposed to physiological pressures and electromechanical stimulation. Similarly, pathophysiological studies using healthy and diseased human cells that may respond positively to ventricular assist should also be conducted. These future experiments, using systems like ours to evaluate hiPSC-CM tissue formation and electromechanical integration within biosynthetic scaffolds, will inform regenerative medicine practices that aim to restore myocardial function[63,76,77].

A direct comparison of engineered ventricle chamber contractile performance with those of ex vivo animal studies is challenging. For example, our thin-wall chambers powered by immature cardiomyocytes generated small differences in chamber pressure (~50 μmHg) and chamber volume (1–5 μl), equivalent to ejection fractions of ~0.2–1.0%, which are smaller than expected for healthy mammalian ventricles by factors of roughly 50–250. Similarly, the contractile work performed by our ventricles (W_S ~ 0.05–0.25 mmHg × μL, or W_S ~ 7–35 nJ) was less than mouse, rat or human left ventricles by factors of ~10^4, 10^5 and 10^8, respectively[24]. Contractile work in our ventricle models was measured using conductance catheters and was smaller than reported for cardiac organoid chambers based on NRVMs[26] or pluripotent hES2 human embryonic stem cell-derived cardiomyocytes[29], where volume changes were indirectly assessed from video recordings. Both types of model cardiac chambers generated similarly shaped elliptical PV loops (Fig. 3b and Supplementary Fig. 14), which are expected from ventricles contracting in the absence of valves and show similarities to PV loops obtained from patients with severe valvular insufficiencies[78]. Our use of conductance catheters was advantageous for direct volume readouts but electrical pacing during catheterization was not recommended by the catheter manufacturer and therefore not performed in these studies. Thus, the positive inotropic effects of isoproterenol observed by others during electrical pacing[29] was not observed by us when isoproterenol was administered to spontaneously beating model ventricles (Fig. 3b, right panels). One solution to this challenge may be the use of optogenetics for optical pacing[79]. Scaling of chamber contractile strength with cardiomyocyte number is expected and it is encouraging to note that contractile strength increased in our preliminary extended culture period experiments (Supplementary Fig. 14). Lastly, our structural arrhythmia disease model reaffirmed the importance of building native-like anisotropic tissues that are important for both normal propagation and arrhythmogenesis[33]. Precise anatomical defects applied to our tissue-engineered model ventricles generated stable pinned rotors and spiral waves (Fig. 5, Supplementary Fig. 11, and Supplementary Videos 12 and 13) that have so far not been demonstrated in engineered cardiac chambers.

In summary, our results demonstrate the feasibility of engineering functional scale models of the heart chambers, where tissue assembly is guided by a nanofibrous culture substrate, with implications for multiscale in vitro cardiology assays and regenerative medicine research. We used primary rat cardiomyocytes and human-stem-cell-derived cardiomyocytes because rat is the current industry standard for the study of heart disease in vitro and in vivo, yet the use of human models will be key for personalized medicine. In this respect, we believe it is important to include use of pre-/clinical grade measurement technologies to provide a more seamless transition between in vitro and in vivo models. This will extend patient-specific in vitro assays from individual cells to complete organ models, and our design rules provide a path towards engineering heart chambers with functional performance increasingly comparable to native organs. Taken together, the capability to tissue-engineer functional model ventricles, and the modular bioreactor technologies designed for in situ instrumentation and functional assessment, provide a suitable system for in vitro cardiology studies that increasingly translate to clinical outcomes.

Methods

Scaffold fabrication. *Polymer solutions.* Ventricle scaffold material precursors were PCL (Sigma-Aldrich 440744) and gelatin type A (Sigma-Aldrich G2500) dissolved in a solvent, 1,1,1,3,3,3-hexafluoro-2-propanol (HFIP; Oakwood Chemical 003409).

All materials were used as received without further modifications. A mixture of 75% PCL and 25% gelatin was dissolved at 6% weight/volume in HFIP and stirred for at least 12 h to ensure homogeneous mixing.

Ventricle scaffold fabrication. Ventricle scaffolds were produced by pull spinning[46] (Fig. 1b and Supplementary Fig. 1a) PCL/gelatin nanofibres onto ellipsoidal collection mandrels (half-ellipsoid with radii: $a=b=4.5$ mm, $c=9$ mm; Supplementary Fig. 1b). Pull spinning incorporates a high-speed (up to 45,000 r.p.m.) rotating bristle that dips into a fixed, continuous polymer source and pulls the polymer column into an anisotropic network of non-woven nanofibres. The solution was injected through a needle (18G flat tip; BD Biosciences) at a rate of 0.2 ml min^{-1} for a total duration of 5 min. Bristle rotation rate was 30,000 r.p.m. Ventricle mandrels were connected to a DeWALT DC 720 1/2′′ cordless drill driver rotation operating at 300 r.p.m. and the mandrels were located 20 cm from the polymer source. All pull-spinning fabrication was performed within a chemical fume hood and the relative humidity was between 10 and 20%. Scaffolds were stored in de-ionized water for 48 h and sterilized by overnight exposure to ultraviolet radiation within a tissue culture hood before use. Overnight exposure to ultraviolet radiation was sufficient to prevent bacterial contamination but future work with thicker scaffolds may benefit from more thorough sterilization procedures.

Scaffold structural and biochemical analysis. *X-ray microcomputed tomography.* Microcomputed tomography was performed at Harvard University's Center for Nanoscale Science (CNS). We used an X-Tek HMXST225 system (Nikon Metrology) equipped with a 225 kV microfocus X-ray source with a 3 µm focal spot size. We used an aluminium target and 115 kV accelerating voltage. Image acquisition and reconstruction was performed using the following software suites: InspectX (X-ray imaging and computed tomography acquisition), CT Pro 3D (volume reconstruction), VG Studio MAX 2.2 (3D volume visualization, rendering and analysis) and Amira (3D volume visualization, rendering and analysis).

Scanning electron microscopy. All SEM imaging was done using a field emitting electron microscope (FESEM Ultra Plus, Zeiss) at a voltage of 15 kV to image scaffold and tissue fibre alignment. Before imaging, all samples were sputter coated with 5 nm of platinum/palladium (Pt/Pd) using a Quorum Sputter Coater (EMS 300T D, Quorum Technologies) to reduce charge accumulation and tissue decomposition during imaging. Decellularized human tissue was prepared using a previously published SDS (sodium dodecyl sulfate) profusion protocol[80] and dehydrated in serial ethanol washes. Dehydrated tissues were then dried using a SAMDRI critical point drier (931 Series SAMDRI, Tousimis) before sputter coating to ensure complete removal of interstitial fluids.

Mechanical testing. To measure elastic modulus, we produced sheets of nanofibrous material (Supplementary Figs 1 and 2), collected on flat glass coverslips, using the same pull-spinning conditions as for ventricle chamber production. Square samples were laser cut (10×10 mm) from these sheets and loaded onto 5×5 mm mounting tines for biaxial tensile testing (2.5 N load cells; Biotester, CellScale). A pre-stress of 5 mN was applied before running four biaxial preconditioning cycles at 5% strain rate to 20% strain. Using the original dimensions of the nanofibrous samples, the strain–strain curve was then calculated (same strain rate and strain were used as preconditioning). To replicate in vitro conditions, tensile measurements were performed in PBS at 37 °C.

X-ray photoelectron spectrometry. A K-Alpha X-ray photoelectron spectrometer (XPS) and Advantage software (K-Alpha XPS, Thermo Scientific) was used to evaluate fresh-spun and wetted scaffold composition in time. Pieces of 75/25 PCL/gelatin scaffold (5×5 mm) were wetted in 1 l of ultra-pure water and stored in an incubator at 37 °C for up to 1 week. Fresh-spun and wetted samples removed from the water bath daily were dried for 12 h under vacuum and their composition evaluated using the XPS system ($n=3$ scaffold pieces and XPS measurements per time point, 0–7 d). Briefly, each sample was etched for 30 s at 500 eV to remove surface debris and was survey scanned over a 400 µm^2 spot size. Gelatin content was estimated based on the measured presence of nitrogen in the sample and the amount of solvent (HFIP) was estimated based on the measured presence of fluorine, each normalized to the element's percentage within their respective molecule.

Fourier transform infrared spectroscopy. We used a Bruker FTIR Microscope (Lumos, Bruker) in attenuated total reflection mode to measure the infrared spectra of the nanofibers. Data plotting was conducted with custom software written in MATLAB (MathWorks).

Experimental animals. NRVMs were isolated from two-day-old neonatal CRL: CD (SD) rats, and left ventricle histological preparations were obtained from adult female CRL: CD (SD) rats. All procedures were approved by the Harvard Animal Care and Use Committee and all research personnel handling animals were appropriately qualified and trained by Harvard's Office of Animal Resources, under the direction of the Attending Veterinarian. Pups were euthanized using a method consistent with the recommendations of the 2013 American Veterinary Medical Association (AVMA) Guidelines on Euthanasia for rodents. Care and use of the rats used in this study comply with the 'US Government Principles for the Utilization and Care of Vertebrate Animals Used in Testing, Research, and Training', the Guide for the Care and Use of Laboratory Animals, and the Animal Welfare Act/Regulations. Harvard University, Faculty of Arts and Sciences (FAS) maintains an Institutional Animal Care and Use Committee (IACUC) as required by the Public Health Service (PHS) Policy on Humane Care and Use of Laboratory Animals. All animal protocols must be approved by the IACUC before animals can be ordered.

Cell and tissue culture. *NRVMs.* NRVMs were isolated from two-day-old neonatal CRL: CD (Sprague-Dawley, SD) rats using published methods[64]. All procedures were approved by the Harvard Animal Care and Use Committee. Cells were seeded at a density of three million cells per ventricle, following procedures described below. Standard culture media were used (M199 culture medium supplemented with 0.1 mM MEM nonessential amino acids, 10% heat-inactivated FBS, 10 mM HEPES, 3.5 g l^{-1} glucose, 2 mM L-glutamine, 2 mg l^{-1} vitamin B-12 and 50 U ml^{-1} penicillin). Samples were incubated under standard conditions at 37 °C and 5% CO_2. At 48 h post seeding the media was exchanged with maintenance media (M199 media supplemented as above but with 2% FBS) and was exchanged again every 48 h until use.

hiPSC-CMs. hiPSC-CMs were acquired commercially (lot numbers CB169CL_V1_1M, CB301_CL_v1_1M, CB319CL_V1_1M, CB324CL_V1_1M, CB331CL_V1_4M; Axiogenesis) and cultured according to manufacturer's instructions with slight modifications. Briefly, for each cryovial containing one million viable hiPSC-CMs, three wells of a six-well tissue culture plate were coated with 0.01 µg ml^{-1} fibronectin (BD Biosciences) for 4 h in a 37 °C incubator. According to the manufacturer, Cor.4U cells show typical ventricular-, atrial- and nodal-like action potentials, demonstrating the different Cor.4U subtypes. Cor.4U comprises 60% ventricular cells. Cryovials of Cor.4U hiPSC-CMs were quickly thawed in a 37 °C water bath, re-suspended in 10 ml of complete culture medium provided by the manufacturer supplemented with 5 µl of 10 mg ml^{-1} puromycin, and cultured in fibronectin-coated tissue culture plates at 37 °C and 5% CO_2 for 48 h to eliminate undifferentiated stem cells from the culture. After 48 h, cells were dissociated with 0.25% trypsin and seeded onto ventricular scaffolds.

hiPSC-CM line PGP1-iPSC. To demonstrate in situ hiPSC proliferation and hiPSC-CM differentiation in our nanofibrous scaffolds, we performed preliminary experiments using the human iPSC line PGP1-iPSC, which we have used previously for monolayer muscle thin-film assays[11]. hiPSCs were seeded on the surface of nanofibrous sheets at a density of 10^5 cells cm^{-2} and proliferated to confluence within four days of culture in mTeSR culture medium (Supplementary Fig. 13a, left panels). hiPSC-CM differentiation was then induced by changing media from mTeSR to RPMI/1640+B27-minus insulin with 8 µM CHIR 99021, incubating for two days, and subsequently changing media to RPMI/1640+B27-minus insulin with 5 µM IWR-endo-1, and incubated for another two days. We then maintained the culture with fresh RPMI/1640+B27 media every other day. Tissue contraction was observed following 8–12 d of differentiation, concomitant with early stages of sarcomeric expression and assembly (Supplementary Fig. 13a, middle panels). Contractile synchrony improved during extended culture periods, concomitant with increased sarcomeric assembly and myocardial tissue anisotropy (Supplementary Fig. 13a, right panels). Immunofluorescence staining confirmed 3D infiltration of hiPSC-CMs within our nanofibrous scaffolds, including early stages of z-disk alignment (Supplementary Fig. 13b).

Ventricle seeding. We sterilized ventricle scaffolds by exposure to ultraviolet radiation in a biosafety hood overnight. The following morning, we incubated the ventricle scaffolds with 100 µg ml^{-1} fibronectin (human natural fibronectin, BD Biosciences) in PBS for 90 min, then transferred cells to the scaffold at high density (0.5 ml full media containing 3 M cells) and incubated (37 °C, 5% CO_2) for 90 min. Full media (2 ml) was then added to each well and incubated overnight. Ventricles were then transferred to larger wells, each well containing 5 ml full media and one ventricle, with media refreshed every 48 h until use.

Histochemical staining. Cardiomyocyte infiltration and orientation within tissue-engineered ventricles was visualized by fluorescent staining of actin and sarcomeres. We stained for F-actin fibres and sarcomeric α-actinin as previously described[64]. Briefly, washed samples were fixed in 4% paraformaldehyde for 20 min. To prepare ventricle cross-sections, we first cast gelatin moulds of the ventricular volume by pouring dissolved gelatin (20% w/v) into ventricle-shaped moulds, followed by cooling and removal of the solid gelatin from the mould. We then pulled fixed ventricles over the gelatin mould to ensure that thin-walled ventricles maintained an ellipsoidal shape during cryopreservation. Ventricles (with gelatin interior) were stored in PBS + 30% sucrose solution overnight at 4 °C, then transferred to 50% sucrose/50% optimal cutting temperature (OCT) water-soluble blend of glycols and resins for 24 h at 4 °C. They were then transferred to cryosectioning containers in 100% OCT and stored at 4 °C for 48 h. Samples

were frozen by partial immersion in 2-methylbutane which was, itself, partially immersed in liquid nitrogen. Frozen ventricles were stored at −80 °C until cryosectioning by microtome (Leica). We obtained 30-µm-thick cross-sections that were transferred to glass microscope slides (Superfrost microscope slides, Sigma) and maintained at room temperature for 2 h prior to storage at −80 °C until staining.

Staining and imaging. Ventricle surfaces or cross-sections were permeabilized in 0.5% Triton-X100 for 20 min in PBS at 37 °C, followed by 2 h incubation with 1:200 dilutions of mouse anti-sarcomeric α-actinin monoclonal primary antibody (Sigma-Aldrich, clone EA-53, catalogue number A7811-11UL). Samples were then washed and concurrently incubated with 1:200 dilutions of DAPI (Sigma-Aldrich), phalloidin conjugated to Alexa-Fluor 488 (Invitrogen) and goat anti-mouse secondary antibody conjugated to tetramethylrhodamine for 2 h at room temperature. Imaging was performed using a Zeiss LSM 5 LIVE confocal microscope with a Plan-Neofluar 40×/1.3 oil objective. For long-range myocardium tissues, samples were imaged using an Olympus IX83 microscope with an attached Andor spinning disk confocal system, on LUCPlanFLNPh 20× and 40× objectives, and were recorded on a Hamamatsu Orca Flash 4.0 C11440 at 16 bit depth. Z-stacks were collected over the height of a single myocardium wall, and then sections were spliced together using a standard deviation projection followed by a pairwise stitching algorithm in National Institutes of Health ImageJ. We quantified cell alignment using a metric known as the orientational order parameter (OOP) that ranges from zero (random organization) to one (perfect alignment)[35,54], applied to immunostained F-actin.

Optical mapping experiments. Calcium propagation was monitored using a modified tandem-lens macroscope (Scimedia) equipped with a high-speed camera (MiCAM Ultima, Scimedia), a plan APO 0.63× objective, a collimator (Lumencor) and a 200 mW Mercury lamp (X-Cite exacte, Lumen Dynamics). After two weeks culture in vitro, ventricles were incubated with 2 µM Rhod-2 (Invitrogen) for 30 min at 37 °C, rinsed, and incubated in dye-free media for an additional 15 min at 37 °C before recording. The ventricles were then rinsed with Tyrode's buffer. Recordings were acquired at a frame rate of 200 Hz. Electrical field and point simulation was applied using two platinum electrodes (Sigma-Aldrich) with 20 mm and 1 mm spacing, respectively. The point stimulator was located at 0.5–1.0 mm from the apex of the ventricle with a motorized *xy*-micromanipulator (Zaber Technologies). Electrical pulses were generated with 12 V amplitude and 10 ms duration using a pulse generator (MyoPacer Cell Stimulator, IonOptix). Pacing frequency was 1 Hz for NRVM ventricles and 3 Hz for hiPSC-CM ventricles (3 Hz pacing was required in this case because lower pacing frequencies were obfuscated by spontaneous activity). Post-processing of data was conducted with custom software written in MATLAB (MathWorks). A spatial filter with 3×3 pixels was applied to improve the signal/noise ratio. Activation time of point-stimulated ventricle was calculated as the average time to maximum upstroke slope of pulses when continuously at 1 Hz pacing during in a 5 s recording window. For structural arrhythmia disease modelling, we built four NRVM model ventricles (two healthy and two pre-injured with circular holes of 1 mm diameter), and spontaneous calcium activity was monitored in all cases. Calcium mapping of pre-injured ventricles was done on day 11 but tissue had grown into the injury site, preventing stable rotor pinning. We repeated calcium mapping experiments on day 12 using the two uninjured ventricles. Both showed evidence of spontaneously generated calcium plane-wave propagation but one had greater homogeneity; this favourable sample is reported here. For calcium imaging, tissue-engineered ventricles were placed in a temperature-controlled Petri dish and imaged from above. We first imaged an uninjured NRVM ventricle with 5 ms exposure windows and a 2.5 s recording window. We then used a 1-mm-diameter biopsy punch to perforate the ventricle wall and repeated calcium imaging. Lastly, we perforated the ventricle with a second 1-mm-diameter hole spaced 5 mm from the first hole and repeated calcium imaging. Analysis was done using MiCAM imaging software (BV_Ana, SciMedia) and custom software derived from a publicly available MATLAB-based optical mapping analysis package (Rhythm2014b)[81]. This ventricle was then fixed and stained to evaluate cell coverage by confocal immunofluorescence imaging (Supplementary Fig. 4). Although our model ventricles were placed in temperature-controlled Petri dishes, with a roughly 2D geometry during calcium imaging, we showed that ventricles could be suspended in our bioreactor chambers (Fig. 4), suggesting future compatibility with isolated heart perfusion systems currently used for small animal cardiology.

PV measurements. For PV experiments, we built a total of 20 rat (NRVM) and 10 human (Cor.4U) model ventricles. Of these, 12 rat and 6 human ventricles were selected for catheterization based on the synchrony and amplitude of contraction observed in vitro by eye and microscope. We report data for 8 rat and 4 human ventricles, for which pressure or volume recordings were discernible at each of 7 isoproterenol doses (0.1 nM to 0.1 mM; total experiment duration ~20–30 min). These data include 3 human and 4 rat ventricles, for which both pressure and volume were recorded at each isoproterenol dose (Fig. 3b). Intraventricular pressure and volume were measured simultaneously using a Millar MPVS Ultra single segment foundation system for rats with SPR-869NR rat PV catheters (ADInstruments). Catheter calibration and PV experiments were performed in freshly prepared Tyrode's solution. First, tissue-engineered ventricles were transferred to a 3.5 cm Petri dish mounted on a temperature-controlled stage (Warner Instruments) to maintain 35 °C working temperature. Ventricles were sutured to silicone tubing through which catheters were inserted (Supplementary Fig. 4a). Data acquired at a sampling rate of 2,000 samples per second using manufacturer-supplied acquisition systems (Millar MPVS Ultra, ADInstruments LabChart) and was exported for post-processing with custom Matlab scripts (MathWorks).

Catheter calibration. Catheters were equilibrated at 35 °C before use and calibrated for pressure using a manometer (Meriam M2; Meriam Process Technologies) and volume using manufacturer-supplied cuvettes (Millar P/N 910-1048). We observed a nonlinear conductance–volume catheter response (Supplementary Fig. 4bi), as expected for these systems[82]. We performed separate scaffold-specific calibrations, where cell-free scaffolds were inflated and deflated by manual application of pressure through a solution-filled syringe connected to the ventricle through a junction port. Here, we aimed to validate our use of thin PCL/gelatin scaffold walls in place of polycarbonate cuvettes or murine myocardium for which the system and catheters were designed and optimized[24,82–86]. Volume estimated by calculating the slope of measured conductance versus cuvette volume (Supplementary Fig. 4bi) or by scaffold filling (Supplementary Fig. 4bi) were in good agreement within a relevant working volume range of ~300–600 µl. We then used a precision pressure-driven microfluidic pump (Elveflow OB1, Elvesys) to generate small-amplitude pressure variations applied to a model ventricle scaffold through the extraventricular (assist) channel of our custom-made bioreactor (Supplementary Fig. 5). The bioreactor is described in more detail in Supplementary Figs 8 and 9. By generating successively smaller peak-to-peak pressure sinusoids, we verified that pressure and volume variations generated by our tissue-engineered model ventricles were above the noise floor (Supplementary Figs. 5–7). In some cases, pressure or volume signal noise and drift were reduced by post-processing using Matlab's 'smooth' and 'polyfit' functions (Supplementary Fig. 4C). Pressure and volume signals were normalized by polynomial background subtraction to reduce unwanted signal drift from large datasets, clarifying frequency-domain analysis of ventricle beat rates over these time periods (Supplementary Fig. 5).

β-adrenergic response of tissue-engineered ventricles. The contractile response of tissue-engineered ventricles to increasing concentrations of the β-adrenergic agonist isoproterenol was measured as follows. A 100 mM stock solution of isoproterenol (Sigma-Aldrich) containing 110 µM ascorbic acid (Sigma-Aldrich) and 45 µM EDTA (Sigma-Aldrich) was prepared in Tyrode's solution and stored at −20 °C. Working concentrations were prepared fresh for each experiment by serial tenfold dilution and kept on ice and protected from light during experiments. The engineered tissues were exposed to concentrations of isoproterenol ranging from 1×10^{-10} M to 1×10^{-4} M by cumulative addition of 1.0 log doses every 2 min. Pressure and volume recordings collected from the last 30 s of each measurement interval were converted to the frequency domain by fast Fourier transform using Matlab and beat rates were estimated using Matlab's 'findpeaks' function applied to pressure or volume fast Fourier transform data (Supplementary Fig. 5).

HBR design and fabrication. HBR designs were created using SolidWorks (DS SolidWorks Corporation). HBR components were fabricated by rapid manufacturing providers (Proto Labs) and by the staff of the John A. Paulson School of Engineering and Applied Sciences (SEAS) Scientific Instrument Shop at Harvard University. The HBR body consisted of three separate polycarbonate pieces that were assembled using stainless steel screws and silicone gaskets (Fig. 4a and Supplementary Figs 6 and 7). To increase optical transparency of HBR polycarbonate components, we performed post-fabrication vapour polishing in our laboratory by methylene chloride vapour exposure in a chemical fume hood.

Echocardiography. We acquired echocardiographic images and videos of ventricle contraction using a Vevo 2100 system (VisualSonics) at the Boston Children's Hospital Small Animal Imaging Laboratory (BCH-SAIL). We used a 21 MHz probe (~60 µm resolution, ~1.4 cm imaging depth) coupled to the HBR window through an index-matching gel.

Statistical analysis. For analysis of tissue OOP and beat-rate response to isoproterenol, one-way analysis of variance (ANOVA) between the compositional groups were conducted using SigmaPlot (v13.0, Systat Software). For pairwise comparison, the Tukey test was applied. For all statistical analyses, P values less than 0.05 were considered statistically significant.

Reporting Summary. Further information on experimental design is available in the Nature Research Reporting Summary linked to this article.

Code availability. The custom MATLAB-based optical mapping analysis package is available at http://efimovlab.org/research/resources/rhythm. Custom Matlab scripts used for data smoothing, Fourier transformation and plotting are available upon request.

Data availability. All data generated and analysed during this study are included in the paper and its Supplementary Information.

Received: 30 July 2017; Accepted: 20 June 2018;
Published online: 23 July 2018

References

1. Benam, K. H. et al. Engineered in vitro disease models. *Annu Rev. Pathol.* **10**, 195–262 (2015).
2. Tzatzalos, E., Abilez, O. J., Shukla, P. & Wu, J. C. Engineered heart tissues and induced pluripotent stem cells: macro- and microstructures for disease modeling, drug screening, and translational studies. *Adv. Drug Deliv. Rev.* **96**, 234–244 (2016).
3. Pacher, P., Nagayama, T., Mukhopadhyay, P., Batkai, S. & Kass, D. A. Measurement of cardiac function using pressure–volume conductance catheter technique in mice and rats. *Nat. Protoc.* **3**, 1422–1434 (2008).
4. Ram, R., Mickelsen, D. M., Theodoropoulos, C. & Blaxall, B. C. New approaches in small animal echocardiography: imaging the sounds of silence. *Am. J. Physiol. Heart Circ. Physiol.* **301**, H1765–1780 (2011).
5. Bakermans, A. J. et al. Small animal cardiovascular MR imaging and spectroscopy. *Prog. Nucl. Magn. Reson. Spectrosc.* **88–89**, 1–47 (2015).
6. Chandrasekera, P. C. & Pippin, J. J. The human subject: an integrative animal model for 21st century heart failure research. *Am. J. Transl. Res.* **7**, 1636–1647 (2015).
7. Gloschat, C. R. et al. Arrhythmogenic and metabolic remodelling of failing human heart. *J. Physiol.* **594**, 3963–3980 (2016).
8. Karakikes, I., Ameen, M., Termglinchan, V. & Wu, J. C. Human induced pluripotent stem cell-derived cardiomyocytes: insights into molecular, cellular, and functional phenotypes. *Circ. Res.* **117**, 80–88 (2015).
9. Feric, N. T. & Radisic, M. Maturing human pluripotent stem cell-derived cardiomyocytes in human engineered cardiac tissues. *Adv. Drug Deliv. Rev.* **96**, 110–134 (2016).
10. Eder, A., Vollert, I., Hansen, A. & Eschenhagen, T. Human engineered heart tissue as a model system for drug testing. *Adv. Drug Deliv. Rev.* **96**, 214–224 (2016).
11. Wang, G. et al. Modeling the mitochondrial cardiomyopathy of Barth syndrome with induced pluripotent stem cell and heart-on-chip technologies. *Nat. Med.* **20**, 616–623 (2014).
12. Lind, J. U. et al. Instrumented cardiac microphysiological devices via multimaterial three-dimensional printing. *Nat. Mater.* **16**, 303–308 (2017).
13. Boudou, T. et al. A microfabricated platform to measure and manipulate the mechanics of engineered cardiac microtissues. *Tissue Eng. Part A* **18**, 910–919 (2012).
14. Nunes, S. S. et al. Biowire: a platform for maturation of human pluripotent stem cell-derived cardiomyocytes. *Nat. Methods* **10**, 781–787 (2013).
15. Thavandiran, N. et al. Design and formulation of functional pluripotent stem cell-derived cardiac microtissues. *Proc. Natl Acad. Sci. USA* **110**, E4698–4707 (2013).
16. Mannhardt, I. et al. Human engineered heart tissue: analysis of contractile force. *Stem Cell Rep.* **7**, 29–42 (2016).
17. Huebsch, N. et al. Miniaturized iPS-cell-derived cardiac muscles for physiologically relevant drug response analyses. *Sci. Rep.* **6**, 24726 (2016).
18. Mathur, A. et al. Human iPSC-based cardiac microphysiological system for drug screening applications. *Sci. Rep.* **5**, 8883 (2015).
19. Turnbull, I. C. et al. Advancing functional engineered cardiac tissues toward a preclinical model of human myocardium. *FASEB J.* **28**, 644–654 (2014).
20. Sidorov, V. Y. et al. I-Wire Heart-on-a-Chip I: three-dimensional cardiac tissue constructs for physiology and pharmacology. *Acta Biomater.* **48**, 68–78 (2017).
21. Godier-Furnemont, A. F. G. et al. Physiologic force–frequency response in engineered heart muscle by electromechanical stimulation. *Biomaterials* **60**, 82–91 (2015).
22. Tiburcy, M. et al. Defined engineered human myocardium with advanced maturation for applications in heart failure modelling and repair. *Circulation* **135**, 1832–1847 (2017).
23. Mathur, A., Ma, Z., Loskill, P., Jeeawoody, S. & Healy, K. E. In vitro cardiac tissue models: current status and future prospects. *Adv. Drug Deliv. Rev.* **96**, 203–213 (2016).
24. Pacher, P., Nagayama, T., Mukhopadhyay, P., Batkai, S. & Kass, D. A. Measurement of cardiac function using pressure–volume conductance catheter technique in mice and rats. *Nat. Protoc.* **3**, 1422–1434 (2008).
25. Burkhoff, D., Mirsky, I. & Suga, H. Assessment of systolic and diastolic ventricular properties via pressure–volume analysis: a guide for clinical, translational, and basic researchers. *Am. J. Physiol. Heart Circ. Physiol.* **289**, H501–512 (2005).
26. Lee, E. J., Kim do, E., Azeloglu, E. U. & Costa, K. D. Engineered cardiac organoid chambers: toward a functional biological model ventricle. *Tissue Eng. Part A* **14**, 215–225 (2008).
27. Gonen-Wadmany, M., Gepstein, L. & Seliktar, D. Controlling the cellular organization of tissue-engineered cardiac constructs. *Ann. N. Y. Acad. Sci.* **1015**, 299–311 (2004).
28. Yildirim, Y. et al. Development of a biological ventricular assist device: preliminary data from a small animal model. *Circulation* **116**, I-16–I-23 (2007).
29. Li, R. A. et al. Bioengineering an electro-mechanically functional miniature ventricular heart chamber from human pluripotent stem cells. *Biomaterials* **163**, 116–127 (2018).
30. Costa, K. D., Takayama, Y., McCulloch, A. D. & Covell, J. W. Laminar fiber architecture and three-dimensional systolic mechanics in canine ventricular myocardium. *Am. J. Physiol.* **276**, H595–607 (1999).
31. Arts, T., Costa, K. D., Covell, J. W. & McCulloch, A. D. Relating myocardial laminar architecture to shear strain and muscle fiber orientation. *Am. J. Physiol. Heart Circ. Physiol.* **280**, H2222–2229 (2001).
32. Rohr, S., Scholly, D. M. & Kleber, A. G. Patterned growth of neonatal rat heart cells in culture. Morphological and electrophysiological characterization. *Circ. Res.* **68**, 114–130 (1991).
33. Kleber, A. G. & Rudy, Y. Basic mechanisms of cardiac impulse propagation and associated arrhythmias. *Physiol. Rev.* **84**, 431–488 (2004).
34. Bursac, N., Parker, K. K., Iravanian, S. & Tung, L. Cardiomyocyte cultures with controlled macroscopic anisotropy: a model for functional electrophysiological studies of cardiac muscle. *Circ. Res.* **91**, e45–54 (2002).
35. Feinberg, A. W. et al. Controlling the contractile strength of engineered cardiac muscle by hierarchal tissue architecture. *Biomaterials* **33**, 5732–5741 (2012).
36. Zong, X. et al. Electrospun fine-textured scaffolds for heart tissue constructs. *Biomaterials* **26**, 5330–5338 (2005).
37. Kai, D., Prabhakaran, M. P., Jin, G. & Ramakrishna, S. Guided orientation of cardiomyocytes on electrospun aligned nanofibers for cardiac tissue engineering. *J. Biomed. Mater. Res B Appl. Biomater.* **98**, 379–386 (2011).
38. Kenar, H., Kose, G. T., Toner, M., Kaplan, D. L. & Hasirci, V. A 3D aligned microfibrous myocardial tissue construct cultured under transient perfusion. *Biomaterials* **32**, 5320–5329 (2011).
39. Orlova, Y., Magome, N., Liu, L., Chen, Y. & Agladze, K. Electrospun nanofibers as a tool for architecture control in engineered cardiac tissue. *Biomaterials* **32**, 5615–5624 (2011).
40. Capulli, A. K., MacQueen, L. A., Sheehy, S. P. & Parker, K. K. Fibrous scaffolds for building hearts and heart parts. *Adv. Drug Deliv. Rev.* **96**, 83–102 (2016).
41. Mauck, R. L. et al. Engineering on the straight and narrow: the mechanics of nanofibrous assemblies for fiber-reinforced tissue regeneration. *Tissue Eng. Part B* **15**, 171–193 (2009).
42. Pope, A. J., Sands, G. B., Smaill, B. H. & LeGrice, I. J. Three-dimensional transmural organization of perimysial collagen in the heart. *Am. J. Physiol. Heart C* **295**, 1243–1252 (2008).
43. Sheehy, S. P., Grosberg, A. & Parker, K. K. The contribution of cellular mechanotransduction to cardiomyocyte form and function. *Biomech. Model. Mechanobiol.* **11**, 1227–1239 (2012).
44. Kim, D. H. et al. Nanoscale cues regulate the structure and function of macroscopic cardiac tissue constructs. *Proc. Natl Acad. Sci. USA* **107**, 565–570 (2010).
45. Savadjiev, P. et al. Heart wall myofibers are arranged in minimal surfaces to optimize organ function. *Proc. Natl Acad. Sci. USA* **109**, 9248–9253 (2012).
46. Deravi, L. F. et al. Design and fabrication of fibrous nanomaterials using pull spinning. *Macromol. Mater. Eng.* **302**, 1600404 (2017).
47. Ruoslahti, E. RGD and other recognition sequences for integrins. *Annu Rev. Cell Dev. Biol.* **12**, 697–715 (1996).
48. Katagiri, Y., Brew, S. A. & Ingham, K. C. All six modules of the gelatin-binding domain of fibronectin are required for full affinity. *J. Biol. Chem.* **278**, 11897–11902 (2003).
49. Meiry, G. et al. Evolution of action potential propagation and repolarization in cultured neonatal rat ventricular myocytes. *J. Cardiovasc. Electrophysiol.* **12**, 1269–1277 (2001).
50. Morse, P. M. & Feshbach, H. *Methods of Theoretical Physics* (McGraw-Hill, New York, 1953).
51. Mandegar, M. A. et al. CRISPR interference efficiently induces specific and reversible gene silencing in human iPSCs. *Cell Stem Cell* **18**, 541–553 (2016).
52. Rohr, S., Kucera, J. P. & Kleber, A. G. Slow conduction in cardiac tissue, I: effects of a reduction of excitability versus a reduction of electrical coupling on microconduction. *Circ. Res* **83**, 781–794 (1998).
53. Yang, X. L., Pabon, L. & Murry, C. E. Engineering adolescence maturation of human pluripotent stem cell-derived cardiomyocytes. *Circ. Res.* **114**, 511–523 (2014).
54. Pasqualini, F. S., Sheehy, S. P., Agarwal, A., Aratyn-Schaus, Y. & Parker, K. K. Structural phenotyping of stem cell-derived cardiomyocytes. *Stem Cell Rep.* **4**, 340–347 (2015).

55. Akselrod, S. et al. Power spectrum analysis of heart rate fluctuation: a quantitative probe of beat-to-beat cardiovascular control. *Science* **213**, 220–222 (1981).
56. Fenske, S. et al. Comprehensive multilevel in vivo and in vitro analysis of heart rate fluctuations in mice by ECG telemetry and electrophysiology. *Nat. Protoc.* **11**, 61–86 (2016).
57. Barrett, A. M. & Carter, J. Comparative chronotropic activity of beta-adrenoceptive antagonists. *Br. J. Pharmacol.* **40**, 373–381 (1970).
58. Brito-Martins, M., Harding, S. E. & Ali, N. N. Beta(1)- and beta(2)-adrenoceptor responses in cardiomyocytes derived from human embryonic stem cells: comparison with failing and non-failing adult human heart. *Br. J. Pharmacol.* **153**, 751–759 (2008).
59. Simpson, P. & Savion, S. Differentiation of rat myocytes in single cell cultures with and without proliferating nonmyocardial cells. Cross-striations, ultrastructure, and chronotropic response to isoproterenol. *Circ. Res.* **50**, 101–116 (1982).
60. Moretti, A. et al. Patient-specific induced pluripotent stem-cell models for long-QT syndrome. *N. Engl. J. Med.* **363**, 1397–1409 (2010).
61. Koglin, J., Bohm, M., Vonscheidt, W., Stablein, A. & Erdmann, E. Antiadrenergic effect of carbachol but not of adenosine on contractility in the intact human ventricle in-vivo. *J. Am. Coll. Cardiol.* **23**, 678–683 (1994).
62. Lim, Z. Y., Maskara, B., Aguel, F., Emokpae, R.Jr & Tung, L. Spiral wave attachment to millimeter-sized obstacles. *Circulation* **114**, 2113–2121 (2006).
63. Ogle, B. M. et al. Distilling complexity to advance cardiac tissue engineering. *Sci. Transl. Med.* **8**, 342ps313 (2016).
64. Feinberg, A. W. et al. Muscular thin films for building actuators and powering devices. *Science* **317**, 1366–1370 (2007).
65. Novosel, E. C., Kleinhans, C. & Kluger, P. J. Vascularization is the key challenge in tissue engineering. *Adv. Drug Deliv. Rev.* **63**, 300–311 (2011).
66. Lundberg, M. S., Baldwin, J. T. & Buxton, D. B. Building a bioartificial heart: obstacles and opportunities. *J. Thorac. Cardiovasc. Surg.* **153**, 748–750 (2017).
67. Chaturvedi, R. R. et al. Passive stiffness of myocardium from congenital heart disease and implications for diastole. *Circulation* **121**, 979–988 (2010).
68. Quinn, K. P. et al. Optical metrics of the extracellular matrix predict compositional and mechanical changes after myocardial infarction. *Sci. Rep.* **6**, 35823 (2016).
69. Gonzalez, G. M. et al. Production of synthetic, para-aramid and biopolymer nanofibers by immersion rotary jet-spinning. *Macromol. Mater. Eng.* **302**, 1600365 (2017).
70. Gladman, A. S., Matsumoto, E. A., Nuzzo, R. G., Mahadevan, L. & Lewis, J. A. Biomimetic 4D printing. *Nat. Mater.* **15**, 413–418 (2016).
71. Zimmermann, W. H. et al. Three-dimensional engineered heart tissue from neonatal rat cardiac myocytes. *Biotechnol. Bioeng.* **68**, 106–114 (2000).
72. Germanguz, I. et al. Molecular characterization and functional properties of cardiomyocytes derived from human inducible pluripotent stem cells. *J. Cell Mol. Med.* **15**, 38–51 (2011).
73. Ronaldson-Bouchard, K. et al. Advanced maturation of human cardiac tissue grown from pluripotent stem cells. *Nature* **556**, 239–243 (2018).
74. Endoh, M. Force–frequency relationship in intact mammalian ventricular myocardium: physiological and pathophysiological relevance. *Eur. J. Pharmacol.* **500**, 73–86 (2004).
75. Bai, S. L., Campbell, S. E., Moore, J. A., Morales, M. C. & Gerdes, A. M. Influence of age, growth, and sex on cardiac myocyte size and number in rats. *Anat. Rec.* **226**, 207–212 (1990).
76. Feric, N. T. & Radisic, M. Strategies and challenges to myocardial replacement therapy. *Stem Cells Transl. Med.* **5**, 410–416 (2016).
77. Pecha, S., Eschenhagen, T. & Reichenspurner, H. Myocardial tissue engineering for cardiac repair. *J. Heart Lung Transplant.* **35**, 294–298 (2016).
78. Klabunde, R. E. *Cardiovascular Physiology Concepts* 2nd edn (Lippincott Williams & Wilkins/Wolters Kluwer, Philadelphia, 2012).
79. Park, S. J. et al. Phototactic guidance of a tissue-engineered soft-robotic ray. *Science* **353**, 158–162 (2016).
80. Guyette, J. P. et al. Bioengineering human myocardium on native extracellular matrix. *Circ. Res.* **118**, 56–72 (2016).
81. Laughner, J. I., Ng, F. S., Sulkin, M. S., Arthur, R. M. & Efimov, I. R. Processing and analysis of cardiac optical mapping data obtained with potentiometric dyes. *Am. J. Physiol. Heart C* **303**, H753–H765 (2012).
82. Pearce, J. A., Porterfield, J. E., Larson, E. R., Valvano, J. W. & Feldman, M. D. Accuracy considerations in catheter based estimation of left ventricular volume. *Conf. Proc. IEEE Eng. Med. Biol. Soc.* **2010**, 3556–3558 (2010).
83. Baan, J. et al. Continuous stroke volume and cardiac output from intra-ventricular dimensions obtained with impedance catheter. *Cardiovasc. Res.* **15**, 328–334 (1981).
84. Baan, J. et al. Continuous measurement of left ventricular volume in animals and humans by conductance catheter. *Circulation* **70**, 812–823 (1984).
85. Raghavan, K. et al. Electrical conductivity and permittivity of murine myocardium. *IEEE Trans. Biomed. Eng.* **56**, 2044–2053 (2009).
86. Clark, J. E. & Marber, M. S. Advancements in pressure–volume catheter technology—stress remodelling after infarction. *Exp. Physiol.* **98**, 614–621 (2013).

Acknowledgements

This work was sponsored by the John A. Paulson School of Engineering and Applied Sciences at Harvard University, the Wyss Institute for Biologically Inspired Engineering at Harvard University, Harvard Materials Research Science and Engineering Center grant DMR-1420570, Defense Threat Reduction Agency (DTRA) subcontract #312659 from Los Alamos National Laboratory under a prime DTRA contract no. DE-AC52-06NA25396, and the National Center for Advancing Translational Sciences of the National Institutes of Health under Award Numbers UH3TR000522 and 1-UG3-HL-141798-01. The content is solely the responsibility of the authors and does not necessarily represent the official views of the National Institutes of Health. This work was supported in part by the US Army Research Laboratory and the US Army Research Office under Contract No. W911NF-12-2-0036. The views and conclusions contained in this document are those of the authors and should not be interpreted as representing the official policies, either expressed or implied, of the Army Research Office, Army Research Laboratory, or the US government. The US government is authorized to reproduce and distribute reprints for government purposes notwithstanding any copyright notation hereon. This work was performed in part at the Center for Nanoscale Systems (CNS), a member of the National Nanotechnology Coordinated Infrastructure Network (NNCI), which is supported by the National Science Foundation under NSF award no. 1541959. CNS is part of Harvard University. We thank M. McKenna and the staff at Harvard University's John A. Paulson School of Engineering and Applied Sciences Scientific Instrument Shop for manufacturing heart bioreactor and nanofibre production system components. We thank M. Griswold and A. Cho for technical assistance, J. Guyette and H. Ott for providing decellularized human left ventricle myocardial tissue samples, E. Snay for assistance with echocardiographic imaging at the Boston Children's Hospital Small Animal Imaging Laboratory, and M. Rosnach for assistance with photography and illustrations. We thank A. Kleber for his expertise and insightful discussions.

Author contributions

L.A.M. and K.K.P. conceived the ideas and designed the experiments. L.A.M., S.P.S., C.O.C., J.F.Z., F.S.P., X.L., J.A.G., P.H.C., G.M.G., S.-J.P., A.K.C., J.P.F. and T.F.K conducted the experiments and analysed the data. L.M. derived the scaling laws. L.A.M., W.T.P. and K.K.P interpreted the data. L.A.M., S.P.S. and K.K.P. wrote the manuscript.

Competing interests

The authors declare no competing interests.

Additional information

Supplementary information is available for this paper at https://doi.org/10.1038/s41551-018-0271-5.

Correspondence and requests for materials should be addressed to K.K.P.

nature research

Corresponding author(s): Kevin Kit Parker

☐ Initial submission ☐ Revised version ☒ Final submission

Life Sciences Reporting Summary

Nature Research wishes to improve the reproducibility of the work that we publish. This form is intended for publication with all accepted life science papers and provides structure for consistency and transparency in reporting. Every life science submission will use this form; some list items might not apply to an individual manuscript, but all fields must be completed for clarity.

For further information on the points included in this form, see Reporting Life Sciences Research. For further information on Nature Research policies, including our data availability policy, see Authors & Referees and the Editorial Policy Checklist.

Experimental design

1. Sample size

Describe how sample size was determined.

Given the absence of prior data on human tissue-engineered ventricles, a statistical determination of sample size was not possible. Instead, we chose a sample size (n=4) compatible with existing datasets relative to contractility assays powered by the same commercially available line of hiPS-CMs. We confirmed this choice by power analysis, which indicated that a sample size of N=4 was sufficient, assuming a 30% increase in beat rate across all groups and a 10% variance.

2. Data exclusions

Describe any data exclusions.

Data was included for analysis if pressure or volume recordings were discernible at each isoproterenol dose (total experiment duration, ~20-30 minutes). Pressure–volume loops and stroke-work analysis required that both pressure and volume recordings were discernible at each isoproterenol dose. Approximately 50% of cultured ventricles (rat or human) produced pressure or volume differences that were measurable by catheterization. Of these, approximately 50% contracted with sufficient stability to conduct isoproterenol dose–response experiments.
In total, we built 20 rat (neonatal rat ventricular myocyte) and 10 human (Cor.4U) model ventricles, from which we obtained pressure–volume data as a function of isoproterenol from 8 rat and 4 human model ventricles.

3. Replication

Describe whether the experimental findings were reliably reproduced.

We observed the expected biological difference in baseline recordings from the ventricles, that is, a distinct spontaneous beating rate. However, the pharmacological response was repeatable. Following isoproterenol exposure, seven out of eight rat ventricles showed positive chronotropy, whereas one ventricle showed a negligible response. For human ventricles, three out of four showed positive chronotropy, whereas the fourth showed mild negative chronotropy.

4. Randomization

Describe how samples/organisms/participants were allocated into experimental groups.

We built a total of 20 rat (neonatal rat ventricular myocyte) and 10 human (Cor.4U) model ventricles. Of these, 12 rat and 6 human ventricles were selected for catheterization on the basis of the synchrony and amplitude of contraction observed in vitro by eye and microscope. We report data for 8 rat and 4 human ventricles, for which pressure or volume recordings were discernible at each of 7 isoproterenol doses (0.1 nM to 0.1 mM; total experiment duration, ~20-30 minutes). These data include 3 human and 4 rat ventricles, for which both pressure and volume were recorded at each isoproterenol dose.

For arrhythmia injury models, we built 4 NRVM model ventricles: 2 healthy and 2 pre-injured. Calcium mapping of pre-injured ventricles was done on day 11 but tissue had grown into the injury site, preventing stable-rotor pinning. We repeated calcium mapping experiments on day 12 using the two uninjured ventricles. Both showed evidence of spontaneously generated calcium plane-wave propagation but one had significantly greater homogeneity; this favorable sample is reported in our revised manuscript. Injuries were applied to this model ventricle following pre-injury recordings.

5. Blinding

Describe whether the investigators were blinded to group allocation during data collection and/or analysis.

Blinding was not performed because experiments were performed in a single setting, and data analysis was automated using commercial software.

Note: all studies involving animals and/or human research participants must disclose whether blinding and randomization were used.

6. Statistical parameters

For all figures and tables that use statistical methods, confirm that the following items are present in relevant figure legends (or in the Methods section if additional space is needed).

n/a	Confirmed
☐	☒ The exact sample size (*n*) for each experimental group/condition, given as a discrete number and unit of measurement (animals, litters, cultures, etc.)
☐	☒ A description of how samples were collected, noting whether measurements were taken from distinct samples or whether the same sample was measured repeatedly
☐	☒ A statement indicating how many times each experiment was replicated
☐	☒ The statistical test(s) used and whether they are one- or two-sided (note: only common tests should be described solely by name; more complex techniques should be described in the Methods section)
☐	☒ A description of any assumptions or corrections, such as an adjustment for multiple comparisons
☐	☒ The test results (e.g. *P* values) given as exact values whenever possible and with confidence intervals noted
☐	☒ A clear description of statistics including central tendency (e.g. median, mean) and variation (e.g. standard deviation, interquartile range)
☐	☒ Clearly defined error bars

See the web collection on statistics for biologists for further resources and guidance.

Software

Policy information about availability of computer code

7. Software

Describe the software used to analyze the data in this study.

Statistical analysis was performed using SigmaPlot (v13.0, Systat Software Inc.). Pressure–volume data was acquired using manufacturer-supplied acquisition software (LabChart v7.3, ADInstruments) and was exported for post-processing with Matlab import routines (Matlab R2016a, MathWorks). We used InspectX and CT Pro 3D (Nikon metrology) for X-ray imaging, CT acquisition and volume reconstruction. We used VG Studio MAX 2.2 (Volume Graphics) and Amira 6.0 (ThermoFisher Scientific) for 3D-volume visualization, rendering and analysis. Calcium imaging and analysis was done using MiCAM imaging software (BV_Ana, SciMedia) and a custom MATLAB-based optical mapping analysis package (Rhythm2014b), publicly available at https://code.google.com/archive/p/rhythm-analysis-software

For manuscripts utilizing custom algorithms or software that are central to the paper but not yet described in the published literature, software must be made available to editors and reviewers upon request. We strongly encourage code deposition in a community repository (e.g. GitHub). *Nature Methods* guidance for providing algorithms and software for publication provides further information on this topic.

Materials and reagents

Policy information about availability of materials

8. Materials availability

Indicate whether there are restrictions on availability of unique materials or if these materials are only available for distribution by a for-profit company.

No unique materials were used.

9. Antibodies

Describe the antibodies used and how they were validated for use in the system under study (i.e. assay and species).

We used standard antibodies validated by the manufacturers. Monoclonal anti-α-actinin (sarcomeric) antibodies produced in mouse were obtained from Sigma-Aldrich (clone EA-53, catalog number A7811-100UL). For secondary antibodies, we used goat anti-Mouse IgG (H+L) Highly Cross-Adsorbed Secondary Antibody, Alexa Fluor Plus 488 (ThermoFisher Cat#A32723) and Alexa Fluor Plus 647 (ThermoFisher Cat#A32728).

10. Eukaryotic cell lines

a. State the source of each eukaryotic cell line used.

Neonatal rat ventricular myocytes were isolated from 2-day old Sprague-Dawley using published methods. Human induced pluripotent stem cell-derived cardiomyocytes (hiPSC-CM) were acquired commercially (Cell-type: Cor.4U, Lot numbers CB169CL_V1_1M, CB301_CL_v1_1M, CB319CL_V1_1M, CB324CL_V1_1M, CB331CL_V1_4M; Axiogenesis, Cologne, Germany). For preliminary in situ hiPSC-CM differentiation, we used cell-type PGP1-iPSC (GM23338; Church lab/Coriell Institute GM23338).

b. Describe the method of cell line authentication used.

Cell viability, sterility, and behavior were authenticated by the vendor.

c. Report whether the cell lines were tested for mycoplasma contamination.

Cells tested negative for mycoplasma contamination as specified by the provider.

d. If any of the cell lines used are listed in the database of commonly misidentified cell lines maintained by ICLAC, provide a scientific rationale for their use.

No commonly misidentified cell lines were used.

Animals and human research participants

Policy information about studies involving animals; when reporting animal research, follow the ARRIVE guidelines

11. Description of research animals

Provide details on animals and/or animal-derived materials used in the study.

Neonatal rat ventricular myocytes were isolated from 2-day old Sprague-Dawley using published methods. For histology, we obtained hearts from adult female Sprague-Dawley rats. All procedures were approved by the Harvard Animal Care and Use Committee.

Policy information about studies involving human research participants

12. Description of human research participants

Describe the covariate-relevant population characteristics of the human research participants.

The study did not involve human research participants.